Pergamon

Int. J. Multiphase Flow Vol. 24, No. 3, pp. 479–498, 1998

Printed in Great Britain
PII: S0301-9322(97)00069-4
0301-9322/98 $19.00 + 0.00

NUMERICAL STUDY OF THE BEHAVIOR OF A BUBBLE ATTACHED TO A TIP IN A NONUNIFORM ELECTRIC FIELD

H. J. CHO[1], I. S. KANG[2], Y. C. KWEON[3] and M. H. KIM[3]

[1]Advanced Fluids Engineering Research Center
[2]Department of Chemical Engineering, POSTECH
[3]Department of Mechanical Engineering, POSTECH, San 31, Hyojadong, Pohang, 790–784, Korea

(Received 13 September 1995; in revised form 20 October 1997)

Abstract—In order to investigate the effects of a nonuniform electric field on the behavior of a bubble, a numerical study on the shape of a bubble attached to a conducting tip on a supporting wall is performed. The equilibrium bubble shape is determined by solving the free boundary problem that consists of the governing equation for electric field and the normal stress condition at the bubble surface. A numerically generated composite orthogonal coordinate system is employed to solve the free boundary problem. A bubble on a tip is found to be extended in the direction parallel to the applied electric field. The elongation increases steeply with an increase of the electric field strength and the height of the tip. It is also observed that a highly elongated bubble has a shape with slender waist. The bubble shape obtained from numerical studies are qualitatively similar to the shapes observed in experiments. If the contact radius is maintained during bubble deformation, the contact angle and the aspect ratio increase with the increase of the electric field strength and the tip height. On the other hand, if the contact angle is fixed during bubble deformation, the contact radius decreases as the electric field strength increases. In order to estimate the effect of electric field on the bubble departure volume, the surface tension force and the downward electric force exerted on a bubble are also computed for a bubble of fixed volume under the fixed contact angle condition. The sum of the two forces is found to decrease with increasing strength of nonuniform electric field. This fact suggests that the bubble departure volume decreases in a nonuniform electric field. © 1998 Elsevier Science Ltd. All rights reserved

Key Words: electrohydrodynamics, bubble on a tip, nonuniform electric field, composite orthogonal coordinate system, bubble departure volume

1. INTRODUCTION

In recent years, the importance of electrohydrodynamic (EHD) enhancement of heat transfer in the boiling process has been widely recognized by the heat transfer community. Among various phenomena related to the EHD heat transfer enhancement, bubble dynamics modification is of great interest and has been the subject of many studies, because the effects of electric field on the heat transfer rate can be best understood in terms of bubble departure volume and frequency. The studies for the effects of electric field on the dynamics of a bubble attached to a surface can be largely classified into two groups based on the nature of the applied electric field: (i) the studies on the effects of uniform electric field, and (ii) the studies on the effects of nonuniform electric field, by uniform or nonuniform electric field, in the present work, we mean an electric field that is uniform or nonuniform in the absence of a bubble).

The effects of a uniform electric field has received relatively minor attention probably because of its inapplicability to industrial evaporators, thus, only a few previous works have been reported. By using the spheroidal approximation on the shape of a bubble, Cheng and Chaddock (1986) investigated the effects of a uniform electric field on the bubble departure size. In order to obtain steady bubble shapes, they extended Fritz's analysis on the maximum bubble volume to the boiling process in the presence of an electric field. In the experiments on the bubble behavior under DC electric field, Ogata and Yabe (1993) observed a horizontal bubble motion on the heating surface and enlargement of the area between the bubble and the heating surface. They analyzed the behavior by considering the electric force exerted on the spheroidally approximated bubble surface. Recently, Cho *et al.* (1996) performed numerical analyses and

experiments on the behavior of a bubble attached to a wall in a uniform electric field under the isothermal condition. They computed numerically the equilibrium shapes of a bubble without making approximation on the bubble shape. Since the contact radius and the contact angle cannot be specified simultaneously at the contact line between a bubble and a solid surface, they considered two distinct cases: (i) the case in which the contact radius is specified while the contact angle varies with deformation, and (ii) the case in which the contact angle is specified while the contact radius varies with deformation. From the numerical results for the case of fixed contact radius condition, they found that the contact angle and the aspect ratio increase with an increase of the electric field strength. They also estimated the bubble departure volume by using the equilibrium force balance at the contact point under the fixed contact angle condition with the expectation that the situation is well described by the fixed contact angle condition. From the analyses, it was found that the applied uniform electric field does not have a significant effect on the bubble departure volume. This fact has been verified by the experimental observation that the bubble departure volume remains nearly constant under the isothermal condition even though the strength of the applied uniform electric field increases.

In contrast to the case of uniform electric field, great efforts have been made to study the mechanisms of boiling heat transfer enhancement in a nonuniform electric field. However, due to the complexity of the electrohydrodynamic phenomena involved, theoretical works are very few and the majority are experimental studies (Watson 1961; Edkie 1976; Karayiannis *et al.* 1988; Ogata *et al.* 1992. Of course, there has been a macroscopic explanation based on the concept of the dielectrophoretic force (Pohl 1958). In a nonuniform electric field, a net force acts on a bubble due to the combined effect of the different permittivities between the liquid and gas phases and the gradient of the square of the electric field. This force attracts a bubble toward the region of weaker electric field no matter of its polarity. In a typical pool boiling system that consists of a heated wire and a surrounding cylindrical electrode, this force tends to pull bubbles off from the heated wire surface more rapidly. Indeed, it has been observed that more bubbles of smaller size depart from the heating surface due to a nonuniform electric field and that the heat transfer is enhanced (Bonjour and Verdier 1960; Markels and Durfee 1964; Baboi *et al.* 1968; Schnurmann and Lardge 1973; Jones 1978). Based on these experimental observations, it is believed that an imposed nonuniform electric field leads to modified bubble dynamics, which in turn promotes boiling heat transfer.

The above macroscopic theory is, however, far from being satisfactory. The theory may be applied to the suspended bubbles in liquid medium, but that is not the case for the bubbles attached to solid wall. Since the theory has been developed based on the volume average concept, it cannot be applied to the bubbles on the boundary. Thus, the promising augmentation technique still awaits more satisfactory understanding on the fundamental mechanism. As mentioned above, the intrinsic complexity of boiling process has hindered the theoretical development for the electrohydrodynamic phenomena. Even in theoretically oriented works, which have been available thus far, the correlation of experimental data takes the major part (Choi 1962; Johnson 1968; Lovenguth and Hanesian 1971; Berghmans 1976; Cooper 1990). Therefore, detailed knowledge of behavior of a bubble, which is attached to a solid wall in the presence of a nonuniform electric field, is necessary to clarify the basic mechanisms of electrohydrodynamic boiling process.

In this present study, a first attempt in this general direction, numerical analyses are performed to investigate the effects of a nonuniform electric field on the static deformation characteristics of a bubble attached to a solid surface in isothermal conditions. As a model problem that involves axisymmetric nonuniform electric field, a cylindrical conducting tip on a supporting wall is considered. As will be shown later, the electric field is strongly converged near the conducting tip and a nonuniform electric field is formed.

The relevance of this work to the electrohydrodynamic boiling process may be found from the fact that the effects of electric field on the bubble departure volume can be estimated by considering only the static behaviors as long as the bubble growth is slow. Therefore, in the later part of this work, the surface tension force and the downward electric force exerted on the bubble surface will be computed under the fixed contact angle condition to estimate the effects on the departure volume with the assumption of slow growth. Although the problems are differ-

ent, there exist some previous works which may justify the estimation of departure volume by considering only the static situation (Oğuz and Prosperetti 1993; Longuet-Higgins *et al.* 1991). Oğuz and Prosperetti considered the dynamics of bubble growth and detachment from a needle (in the absence of electric field) by using an approximate model and a full numerical model based on a boundary-integral potential flow calculations. As part of the full numerical results, they showed explicitly that the departure volume is nearly independent of growth rate if the growth rate is less than the critical value. Although the problem is different from the present one in that they computed the departure volume by using the fixed contact radius condition in the absence of electric field, their results clearly show that the dynamical contribution is negligible as long as the growth is slow.

2. PROBLEM STATEMENT

In order to study the effects of a nonuniform electric field on the deformation of a bubble in a liquid, we consider a gas bubble attached to a tip on a wall as shown in figure 1. The conducting tip electrode is a cylinder of height h and radius w, and is assumed to be supported by two types of bottom wall: a conducting wall and an insulating wall. In the figure, x and σ are the symmetry axis and the radial coordinate of the cylindrical coordinate system, and r and θ are the coordinate variables in the spherical coordinate system. The origin is located at the center of the bottom of bubble, and thus $r = (x^2+\sigma^2)^{1/2}$. For convenience in analysis, we divide the problem domain into two parts: the subdomain (I) where $x>0$, and the subdomain (II) where $-h \le x \le 0$, $w \le \sigma < \infty$.

The system is assumed to be under isothermal conditions so that the properties of the surrounding liquid and gas inside the bubble are uniform. The bubble volume is assumed to be $2\pi a^3/3$, where a is the radius of an equivalent hemispherical bubble attached to a tip. The bubble surface is assumed to be characterized by the surface tension γ and the bubble is assumed to sit on the conducting tip with contact angle θ_c and contact radius r_c. In our numerical studies, the bubble volume and the contact radius are assumed to be maintained during bubble deformation. The electrical conductivity and permittivity of the gas inside the bubble are assumed to be negligible in comparison with those of the surrounding liquid. It is also assumed that there is no bulk free charge in the surrounding incompressible liquid. The applied electric field far from the bubble is given by $\mathbf{E}_\infty = -E_\infty \mathbf{e}_x$. In terms of the electric potential, which is defined by $\mathbf{E}_\infty = -\nabla\phi_\infty$, the far field is given by

$$\phi_\infty = E_\infty(x+h). \qquad [1]$$

As mentioned above, it is assumed that there is no bulk free charge in the surrounding liquid. Therefore, the electric potential satisfies the Laplace equation

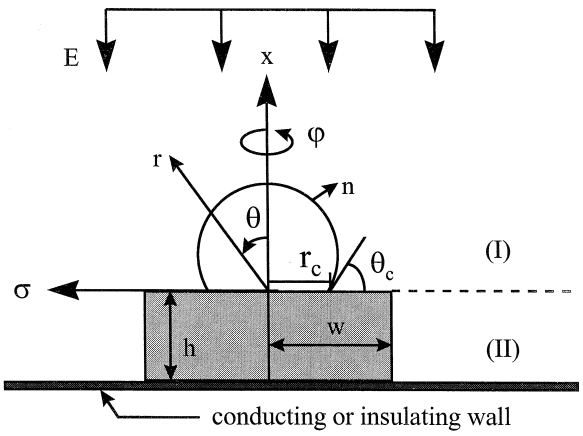

Figure 1. A schematic for a bubble attached to a conducting tip on a wall in a nonuniform electric field..

$$\nabla^2\phi = 0. \quad [2]$$

The boundary conditions at the bubble and tip surfaces are

$$\phi \rightarrow E_\infty(x+h) \quad \text{as } r\rightarrow\infty, \quad [3]$$

$$\mathbf{n}\cdot\nabla\phi = 0 \quad \text{on the bubble surface}, \quad [4]$$

$$\phi = 0 \quad \text{for } x = 0,\ r_c \le \sigma \le w, \quad [5]$$

$$\phi = 0 \quad \text{for } \sigma = w,\ -h \le x \le 0, \quad [6]$$

$$\phi \rightarrow E_\infty(x+h) \quad \text{for } -h \le x \le 0,\ \sigma\rightarrow\infty, \quad [7]$$

where $\mathbf{n}$ is the outgoing unit normal vector from the bubble surface. The boundary condition at the bottom wall ($x = -h$, $w \le \sigma < \infty$) is

$$\phi = 0 \quad \text{for conducting wall}, \quad [8]$$

or

$$\mathbf{e}_x\cdot\nabla\phi = 0 \quad \text{for insulating wall}. \quad [9]$$

Equation [4] is the condition that the normal component of the current vector vanishes at the insulating interface. Equations [5] and [6] are the conditions that the surface potential of a conducting tip electrode must be uniform.

The bubble shape is determined by the normal stress condition, which can be simplified to

$$-(p_{\text{out}} - p_{\text{in}}) + \mathbf{n}\cdot(\mathbf{n}\cdot\mathbf{T}^e)_{\text{out}} = \gamma(\nabla\cdot\mathbf{n}), \quad [10]$$

under the assumption that the electrical conductivity and permittivity of the gas inside the bubble are negligible in comparison with those of the surrounding liquid. Under the given assumption, $\mathbf{n}\cdot(\mathbf{n}\cdot\mathbf{T}^e)_{\text{in}}$ is negligible compared with $\mathbf{n}\cdot(\mathbf{n}\cdot\mathbf{T}^e)_{\text{out}}$. In [10], p_{out} is the pressure simply redefined by addition of an electrically induced pressure based on the incompressibility assumption for the surrounding liquid. The Maxwell stress tensor $\mathbf{T}^e$ is given by

$$\mathbf{T}^e = \epsilon\mathbf{E}\mathbf{E} - \tfrac{1}{2}\epsilon E^2\mathbf{I}, \quad [11]$$

where ϵ is the electrical permittivity and E is the magnitude of $\mathbf{E}$. By using the condition $E_{\text{n}} = \mathbf{n}\cdot\nabla\phi = 0$ at the bubble surface, the normal stress condition can be written as

$$-\Delta p_0 + \Delta\rho g x - \tfrac{1}{2}\epsilon E_t^2 = \gamma(\nabla\cdot\mathbf{n}), \quad [12]$$

where Δp_0 is the pressure difference at $x = 0$, $\Delta\rho$ the density difference, and E_{t} the tangential component of the electric field.

The contact condition of a bubble to the solid surface has not been fully established yet. Nevertheless, we need to specify the condition in order to make the problem determinate. In the present work, we have considered two distinct cases: (i) the case in which the contact radius is specified while the contact angle varies with bubble deformation, and (ii) the case in which the contact angle is specified while the contact radius varies with bubble deformation.

To non-dimensionalize the governing equations and boundary conditions, we introduce the following characteristic scales

$$l_c = a, \qquad \phi_c = E_\infty l_c. \quad [13]$$

Then the dimensionless governing equation and boundary conditions are (we adopt the same notations for the dimensionless variables as dimensional ones if not confused)

$$\nabla^2\phi = 0, \quad [14]$$

with

$$\phi \to x + H \quad \text{as } r \to \infty, \tag{15}$$

$$\mathbf{n} \cdot \nabla\phi = 0 \quad \text{on the bubble surface,} \tag{16}$$

$$\phi = 0 \quad \text{for } x = 0,\ R_c \le \sigma \le W, \tag{17}$$

$$\phi = 0 \quad \text{for } \sigma = W,\ -H \le x \le 0, \tag{18}$$

$$\phi \to x + H \quad \text{at } -H \le x \le 0,\ \sigma \to \infty, \tag{19}$$

$$\begin{aligned} \phi = 0 \text{ (conducting wall)} \quad &\text{for } x = -H,\ W \le \sigma < \infty, \\ \mathbf{e}_x \cdot \nabla\sigma = 0 \text{ (insulating wall)} \quad &\text{for } x = -H,\ W \le \sigma < \infty, \end{aligned} \tag{20}$$

where H and W are the dimensionless tip lengths defined by $H = h/a$, $W = w/a$ and R_c the dimensionless contact radius, r_c/a.

The dimensionless normal stress condition is

$$-N_p + N_g x - \frac{N_e}{2} E_t^2 = (\nabla \cdot \mathbf{n}), \tag{21}$$

where $N_p = \Delta p_0 a/\gamma$ and $N_g = \Delta\rho g a^2/\gamma$. In this present work, the magnitude of electrical stress is assumed to be negligible with respect to the gas pressure inside the bubble. Therefore, the gas inside the bubble is assumed to be incompressible in order to have the condition of a fixed bubble volume. This condition of fixed bubble volume is used to determine the constant N_p. The gravity-capillary number (Crowley 1995). N_g, represents the ratio of gravity force to surface tension force on the bubble surface. In this work, it is assumed that the gravity effect is negligible, that is $N_g \to 0$, based on the observation that the bubble radius ranged from 0.1 mm to 0.3 mm in the experiment of which the results will be shown later. Another dimensionless number of importance in [21] is N_e, which is defined by $N_e = \epsilon E_\infty^2 a/\gamma$ and is called the electrical Weber number. The electrical Weber number Ne is the ratio of the electrical force to the surface tension force. Thus, in general, the bubble deformation increases as Ne increases.

In this work, the free boundary problem defined by [14]–[21] has been solved numerically by using an orthogonal grid generation method.

3. NUMERICAL SCHEME

The domain of the present problem is quite complicated. Thus, for convenience in analysis, we divide it into two parts: the subdomain (I) where $x > 0$, and the subdomain (II) where $-H \le x \le 0$, $W \le \sigma < \infty$. For the subdomains (I) and (II), we define the electrical potentials as $\phi^{(\mathrm{I})}$ and $\phi^{(\mathrm{II})}$, which can be obtained by solving two Laplace's equations with the boundary conditions in [15]–[20] if suitable matching conditions are provided at the interface of two subdomains. The matching conditions at the interface of two subdomains ($x = 0$, $W \le \sigma < \infty$) are

$$\phi^{(\mathrm{I})} = \phi^{(\mathrm{II})} \tag{22}$$

and

$$\frac{\partial\phi^{(\mathrm{I})}}{\partial x} = \frac{\partial\phi^{(\mathrm{II})}}{\partial x}. \tag{23}$$

A composite coordinate system is used for the numerical analysis. The composite coordinate system consists of the boundary-fitted orthogonal curvilinear coordinate system in the subdomain (I) and the simple cylindrical coordinate system in the subdomain (II) as shown in the right part of figure 2. For the free boundary problem in the subdomain (I), the boundary shape must be determined iteratively as part of solution starting from a certain initial shape. We use the method of Ryskin and Leal (1983) for generation of the boundary-fitted orthogonal grid

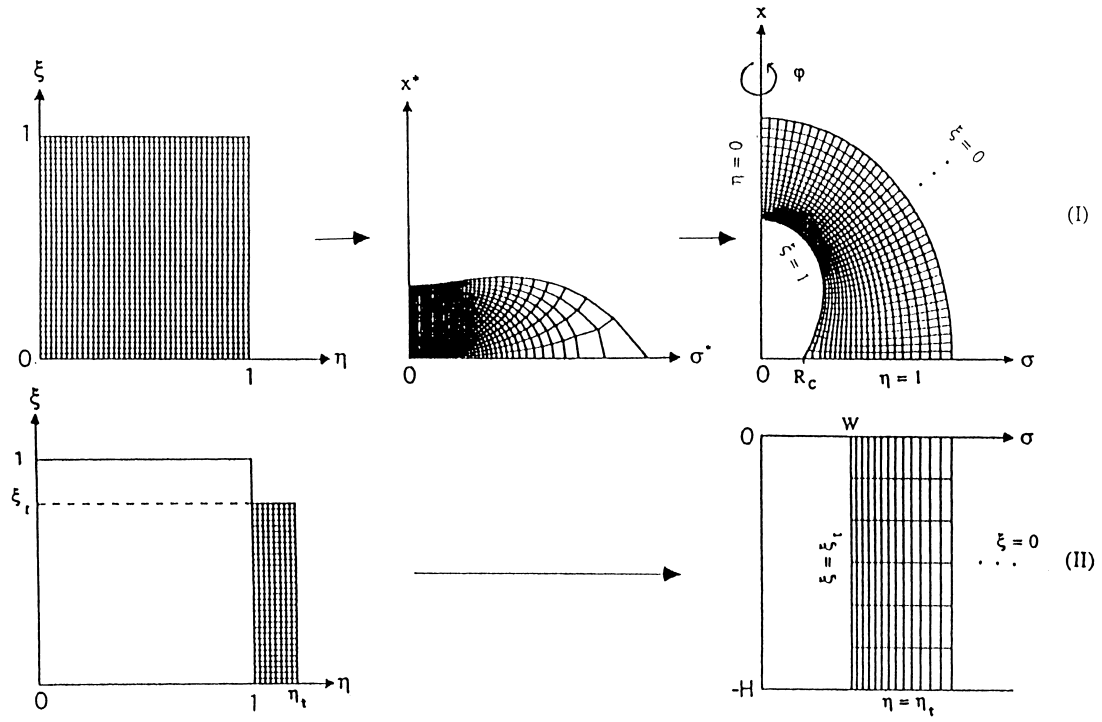

Figure 2. The grid generation scheme of a composite orthogonal coordinate system..

system in the subdomain (I). Their numerical grid generation method has been successfully applied for various free boundary problems in fluid mechanics (Kang and Leal 1987); Noh *et al.* 1993).

In this section, the basic idea of grid generation for a composite coordinate system is briefly introduced. The global numerical scheme to obtain the electric potential with determination of bubble shape in a composite coordinate system will also be presented.

3.1. *Generation of composite grid system*

Numerical generation of a composite grid system in the subdomains (I) and (II) is schematically shown in figure 2. The boundary-fitted orthogonal coordinate system is first generated in the subdomain (I) then the coordinates in (II) are generated.

Since the subdomain (I) is an infinite domain, the inverse conformal mapping

$$x + i\sigma = \frac{1}{x^* - i\sigma^*} \qquad [24]$$

is used to transform the grid generation problem to one in a finite (x^*, σ^*) domain. The orthogonal coordinate mapping between the (x^*, σ^*) domain and the computational domain (ξ, η) is generated by solving the covariant Laplace equations (see Ryskin and Leal (1983), for the details),

$$\frac{\partial}{\partial \xi}\left(f\frac{\partial x^*}{\partial \xi}\right) + \frac{\partial}{\partial \eta}\left(\frac{1}{f}\frac{\partial x^*}{\partial \eta}\right) = 0, \qquad [25]$$

$$\frac{\partial}{\partial \xi}\left(f\frac{\partial \sigma^*}{\partial \xi}\right) + \frac{\partial}{\partial \eta}\left(\frac{1}{f}\frac{\partial \sigma^*}{\partial \eta}\right) = 0, \qquad [26]$$

where $f(\xi, \eta)$ is the distortion function defined as the ratio of two scale factors, that is $f \equiv h_\eta^{(\mathrm{I})}/h_\xi^{(\mathrm{I})}$. For grid generation, we have followed Ryskin and Leal (1984) in which the distortion function is specified as a function of ξ, that is $f = \pi\xi/2$.

The rectangular coordinate system in the subdomain (II) can be easily generated by using the known values of $\sigma(\xi, 1)$ obtained from the orthogonal grid system for subdomain (I). In subdomain (II), the $\xi = const$ lines are simple continuation of $\xi = const$ lines in (I). The $\eta = const$ lines in (II) are equi-distance lines parallel to σ-axis.

3.2. *Governing equation and boundary conditions in composite coordinate system*

As mentioned previously, the solution technique is based upon a numerically generated orthogonal coordinate system. Therefore, we start with the expressions for the governing equation and boundary conditions in such a coordinate system.

In the subdomain (I), the Laplace equation for the electric potential around a bubble $\phi^{(I)}$ is expressed as (Batchelor 1967)

$$\frac{\partial}{\partial\xi}\left(\frac{h_\eta\sigma}{h_\xi}\frac{\partial\phi^{(I)}}{\partial\xi}\right)+\frac{\partial}{\partial\eta}\left(\frac{h_\xi\sigma}{h_\eta}\frac{\partial\phi^{(I)}}{\partial\eta}\right)=0. \qquad [27]$$

In order to avoid the difficulty arising from the singularity at infinity, we define a function ϕ^* as $\phi^* = \phi^{(I)}-\phi_0$, where ϕ_0 is an unbounded function such that $\phi_0 \to x + H$. Therefore we can assume $\phi^* \to 0$ as $r \to \infty$. In this problem, we have used function ϕ_0

$$\phi_0 = \left(\frac{1}{2r^2}+r\right)\cos\,\theta + H = x\left(\frac{1}{2r^3}+1\right)+H. \qquad [28]$$

Using the relation $\phi^{(I)} = \phi^* + \phi_0$, we obtain the governing equation for ϕ^* in orthogonal coordinates

$$\frac{\partial}{\partial\xi}\left(\frac{h_\eta\sigma}{h_\xi}\frac{\partial\phi^*}{\partial\xi}\right)+\frac{\partial}{\partial\eta}\left(\frac{h_\xi\sigma}{h_\eta}\frac{\partial\phi^*}{\partial\eta}\right)=-\frac{\partial}{\partial\xi}\left(\frac{h_\eta\sigma}{h_\xi}\frac{\partial\phi_0}{\partial\xi}\right)-\frac{\partial}{\partial\eta}\left(\frac{h_\xi\sigma}{h_\eta}\frac{\partial\phi_0}{\partial\eta}\right), \qquad [29]$$

with the boundary conditions

$$\phi^* = 0 \quad \text{at } \xi = 0,\ 0\le\eta\le 1, \qquad [30]$$

$$\frac{\partial\phi^*}{\partial\xi} = -\frac{\partial\phi_0}{\partial\xi} \quad \text{at } \xi = 1,\ 0\le\eta\le 1, \qquad [31]$$

$$\frac{\partial\phi^*}{\partial\eta} = -\frac{\partial\phi_0}{\partial\eta} \quad \text{at } \eta = 0,\ 0\le\xi\le 1, \qquad [32]$$

$$\frac{\partial\phi^*}{\partial\eta} = \frac{h_\eta^{(I)}}{h_\eta^{(II)}}\frac{\partial\phi^{(II)}}{\partial\eta}-\frac{\partial\phi_0}{\partial\eta} \quad \text{at } \eta = 1,\ 0\le\xi\le\xi_t, \qquad [33]$$

$$\phi^* = -\phi_0 \quad \text{at } \eta = 1,\ \xi_t\le\xi\le 1, \qquad [34]$$

where [33] is one of the matching conditions [23] at the interface of the subdomains (I) and (II), and ξ_t is the ξ-coordinate value representing the tip position in (ξ, η) domain.

In the subdomain (II), the Laplace equation for the electric potential around a tip $\phi^{(II)}$ is also expressed as

$$\frac{\partial}{\partial\xi}\left(\frac{h_\eta\sigma}{h_\xi}\frac{\partial\phi^{(II)}}{\partial\xi}\right)+\frac{\partial}{\partial\eta}\left(\frac{h_\xi\sigma}{h_\eta}\frac{\partial\phi^{(II)}}{\partial\eta}\right)=0. \qquad [35]$$

The governing equation [35] is solved subject to the boundary conditions

$$\phi^{(II)} = x + H \quad \text{at } \xi = 0,\ 1\le\eta\le\eta_t, \qquad [36]$$

$$\phi^{(\mathrm{II})} = 0 \quad \text{at } \xi = \xi_t,\ 1 \le \eta \le \eta_t, \tag{37}$$

$$\begin{aligned} \phi^{(\mathrm{II})} &= 0 \text{ (conducting wall)} \quad \text{at } \eta = \eta_t,\ 0 \le \xi \le \xi_t, \\ \frac{\partial \phi^{(\mathrm{II})}}{\partial \eta} &= 0 \text{ (insulating wall)} \quad \text{at } \eta = \eta_t,\ 0 \le \xi \le \xi_t, \end{aligned} \tag{38}$$

$$\phi^{(\mathrm{II})} = \phi^{(\mathrm{I})} \quad \text{at } \eta = 1,\ 0 \le \xi \le \xi_t, \tag{39}$$

where [38] is the bottom wall condition, [39] the matching condition at the interface of two subdomains, and η_t the η-coordinate value representing the position of bottom wall in (ξ, η) domain.

To obtain numerical solutions of the governing equations [29] and [35], we have expressed them in a general form as

$$0 = f^2 \frac{\partial^2 \omega}{\partial \xi^2} + \frac{\partial^2 \omega}{\partial \eta^2} + q_1 \frac{\partial \omega}{\partial \xi} + q_2 \frac{\partial \omega}{\partial \eta} + q_3 \omega + q_4, \tag{40}$$

in which ω represents $\phi^{(\mathrm{I})}$ or $\phi^{(\mathrm{II})}$ and q_{i} are coefficients that do not depend on ω. To solve [40], we modified it into a fictitious time-dependent problem and used the ADI method, which can be represented as

$$\frac{\omega^{\nu+1/2} - \omega^{\nu}}{\frac{1}{2}\tau} = f^2 \frac{\delta^2 \omega^{\nu+1/2}}{\delta \xi^2} + \frac{\delta^2 \omega^{\nu}}{\delta \eta^2} + q_1 \frac{\delta \omega^{\nu+1/2}}{\delta \xi} + q_2 \frac{\delta \omega^{\nu}}{\delta \eta} + q_3 \omega^{\nu+1/2} + q_4, \tag{41}$$

$$\frac{\omega^{\nu+1} - \omega^{\nu+1/2}}{\frac{1}{2}\tau} = f^2 \frac{\delta^2 \omega^{\nu+1/2}}{\delta \xi^2} + \frac{\delta^2 \omega^{\nu+1}}{\delta \eta^2} + q_1 \frac{\delta \omega^{\nu+1/2}}{\delta \xi} + q_2 \frac{\delta \omega^{\nu+1}}{\delta \eta} + q_3 \omega^{\nu+1} + q_4, \tag{42}$$

where ν is the iteration number. The fictitious time step size τ is of $O(10^{-3})$ and the convergence criterion is

$$\max |\omega_{i,j}^{\nu+1/2} - \omega_{i,j}^{\nu}| < 10^{-9}.$$

3.3. *Normal stress condition at the free surface*

In order to determine the bubble shape in an electric field, we need to consider the normal stress balance at the bubble surface. When $N_g \to 0$, the normal stress condition [21] reduces to the form

$$-N_p - \frac{N_e}{2} E_\eta^2 - (\kappa_{(\eta)} + \kappa_{(\varphi)}) = 0, \tag{43}$$

where $E_\eta = (1/h_\eta)(\partial \phi / \partial \eta)$, and $\kappa_{(\eta)}$ and $\kappa_{(\varphi)}$ denote the curvatures in the $\mathbf{e}_{(\eta)}$ and $\mathbf{e}_{(\varphi)}$ directions. For the axisymmetric orthogonal coordinate system, the curvatures are given by

$$\kappa_{(\eta)} = \frac{1}{h_\eta^3} \left(\frac{\partial x}{\partial \eta} \frac{\partial^2 \sigma}{\partial \eta^2} - \frac{\partial^2 x}{\partial \eta^2} \frac{\partial \sigma}{\partial \eta} \right), \qquad \kappa_{(\varphi)} = -\frac{1}{h_\eta \sigma} \frac{\partial x}{\partial \eta}. \tag{44}$$

Since we assume that the bubble volume is fixed, the value of N_p in [43] must be determined so as to satisfy the following condition at the bubble surface

$$V = \left| \pi \int_0^1 \left(\sigma^2 \frac{\partial x}{\partial \eta} \right) \mathrm{d}\eta \right| = \text{const.} \tag{45}$$

4. RESULTS AND DISCUSSION

As a reference problem, we have considered an insulating bubble attached directly to a conducting wall ($H = 0$). (In this case, the electric field would be uniform in the absence of the

bubble.) Figure 3(a) shows the equipotential lines around the bubble for the case of $H = 0$, $R_c = 0.6$ and $Ne = 0.1$. As shown in the figure, the equipotential lines become curved near the bubble surface to satisfy the boundary condition $\partial\phi/\partial n = 0$, but the electric field is virtually uniform away from the bubble. For the case of a bubble attached to a tip on a conducting wall, however, figure 3(b) and 3(c) show that the equipotential lines are highly curved in the vicinity of the bubble and the tip. (In this case, the electric field would be nonuniform even if the bubble is absent.) Compared with the case of direct attachment of a bubble to conducting wall (figure 3(a)), we can see that the electric field is much more nonuniform near the bubble. The nonuniformity of electric field extends far from the bubble due to the presence of the tip.

Figure 4 shows the equipotential lines around a bubble attached to a tip on an insulating wall for two values of H. As shown in the figure, the electric potential satisfies the insulating boundary condition at the bubble surface and the supporting wall, $\partial\phi/\partial n = 0$, simultaneously. Therefore, the electric field converges only to the tip. This electric field concentration due to convergence implies that a strongly nonuniform electric field is generated near the bubble and the tip. As the tip height increases, this field concentration effect is added to the effect due to increase of tip height.

From the numerical results on the electric potential distribution, the electric force exerted on the bubble surface can be obtained. In figure 5, the **n**-directional component of the dimensionless electric force, $\mathbf{n}\cdot(\mathbf{n}\cdot\mathbf{T}^e)$ exerted on the bubble surface due to the applied electric field in the case of conducting wall is shown for several values of H. As shown in the figure, the magnitude of electric force has minimum value at the pole of bubble ($\theta = 0^\circ$), and maximum value at the lower side of the bubble ($67.5^\circ \leq \theta \leq 76.5^\circ$). Since the values are negative, the electric field exerts a force inward, (that is $-\mathbf{n}$ direction) or suppress the bubble surface. The bubble deforms inward near $\theta = 70^\circ$ and outward near $\theta = 0^\circ$ to keep the bubble volume constant. The maximum value of the electric force magnitude increases with an increase of the tip height. In consequence, the nonuniform distribution of the electric force becomes stronger as the tip height increases.

The effect of electric field concentration on the electric force exerted on the bubble surface is shown in figure 6 for various values of H. As mentioned earlier, the electric field is concentrated and becomes stronger near the surface of the conducting tip when the bottom wall is insulating. As shown in figure 6, the effect of electric field concentrations due to the insulating bottom wall is prominent when H is small, but the effect decreases as H increases. Therefore, the electric force distribution at the bubble surface is more sensitive to the electric field concentration effect due to insulating bottom wall in the case of smaller tip height. From the numerical results, we can expect that the degree of bubble deformation is largely affected by the nonuniformity of the electric field which depends on the height of the tip and the type of supporting wall.

In figures 7–9, the bubble shape evolution with increasing Ne values under the fixed contact radius condition is shown for the case of a conducting wall. When other parameters are fixed, a bubble becomes more extended as the electric field strength increases. When $H = 0$, the bubble shape does not change much over the entire range of Ne values considered in the study. When

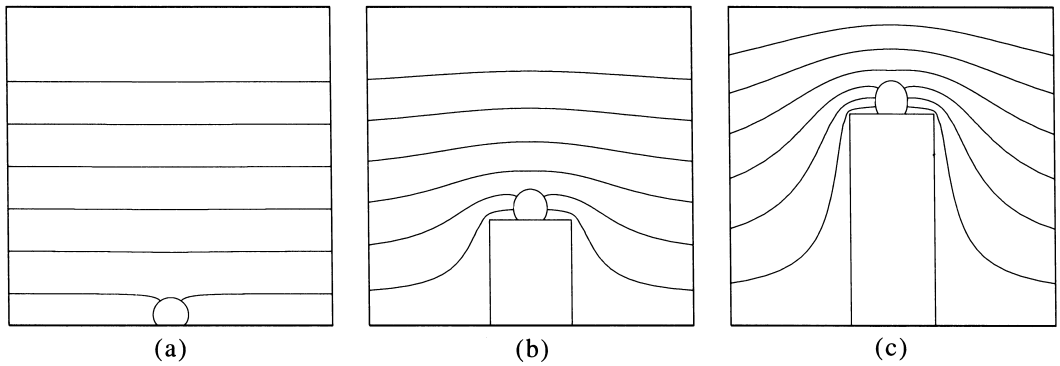

Figure 3. Equipotential lines around a bubble attached to a tip on a conducting wall ($W = 3.2$, $R_c = 0.6$, $N_e = 0.1$): (a) $H = 0$, (b) $H = 5$, (c) $H = 10$..

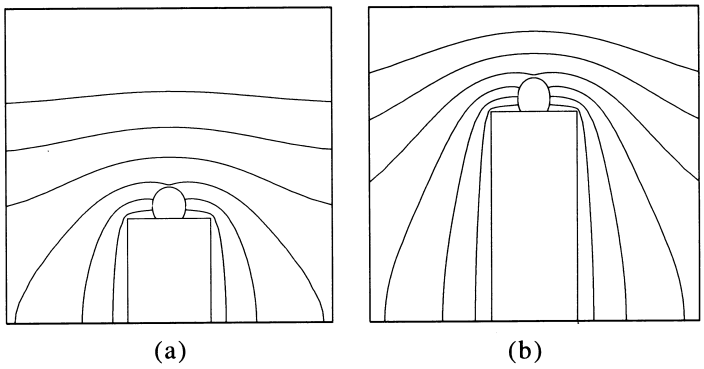

Figure 4. Equipotential lines around a bubble attached to a tip on an insulating wall ($W = 3.2$, $R_c = 0.6$, $N_e = 0.1$): (a) $H = 5$, (b) $H = 10$..

$H > 2$, however, the degree of deformation increases remarkably as Ne increases. For the same value of $Ne (Ne > 0)$, we can see that the degree of deformation increases drastically as H increases. It has also been observed that a bubble on a tip has a slender waist at the lower side when the degree of deformation is very large. This slender waist is believed to be due to the distribution of the electric force at the bubble surface such as the one shown in figure 5.

Figures 10 and 11 show the evolution of bubble shape for the cases of insulating bottom wall. As mentioned earlier, owing to the strongly nonuniform electric field near the bubble in this case, the bubble shape with slender waist can be obtained even at smaller values of Ne compared with the cases of conducting bottom wall (see figures 8 and 9).

The above deformation characteristics may be verified by the experimental observations of Kweon *et al.* (1995). Photographs in figure 12 show the shape of an air bubble attached to a needle electrode: figure 12(a) for the case of the conducting bottom wall, and figure 12(b) for the case of the insulating bottom wall. Since the uniform electric field condition at infinity is not assumed in experiment due to the finite ratio of the electrode gap distance to the needle height, no quantitative comparison with numerical results has not been made. However, we can see that the qualitative deformation characteristics are in good agreement with the numerical results at least in two aspects. Firstly, a highly deformed bubble has a slender waist. Secondly, when the applied electric field strength is the same, the degree of deformation is higher in the case of insulating bottom wall (or plate).

The imposed electric field also affects the contact angle θ_c via bubble deformation. Figure 13(a) shows the dependency of the contact angle on Ne for the case of conducting bottom wall. When $H = 0$, the contact angle remains nearly constant over the whole range of Ne values that are considered. As the height of tip increases, the contact angle increases with increase of Ne

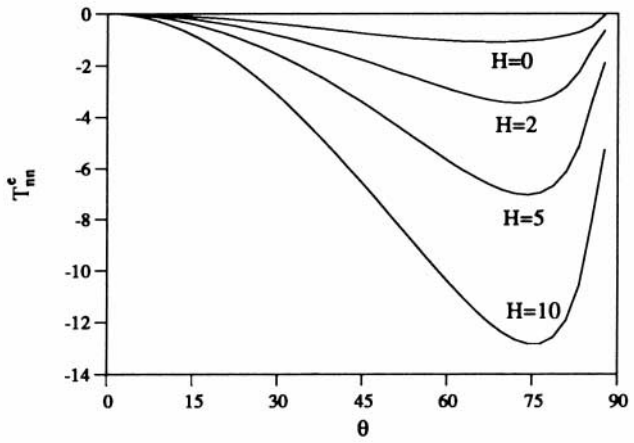

Figure 5. The **n**-directional component of the electric force ($\mathbf{n}\cdot(\mathbf{n}\cdot\mathbf{T}^e)$ in dimensionless form) exerted on the bubble surface in the case of conducting wall for several H values ($W = 3.7$, $R_c = 0.5$, $N_e = 0.1$)..

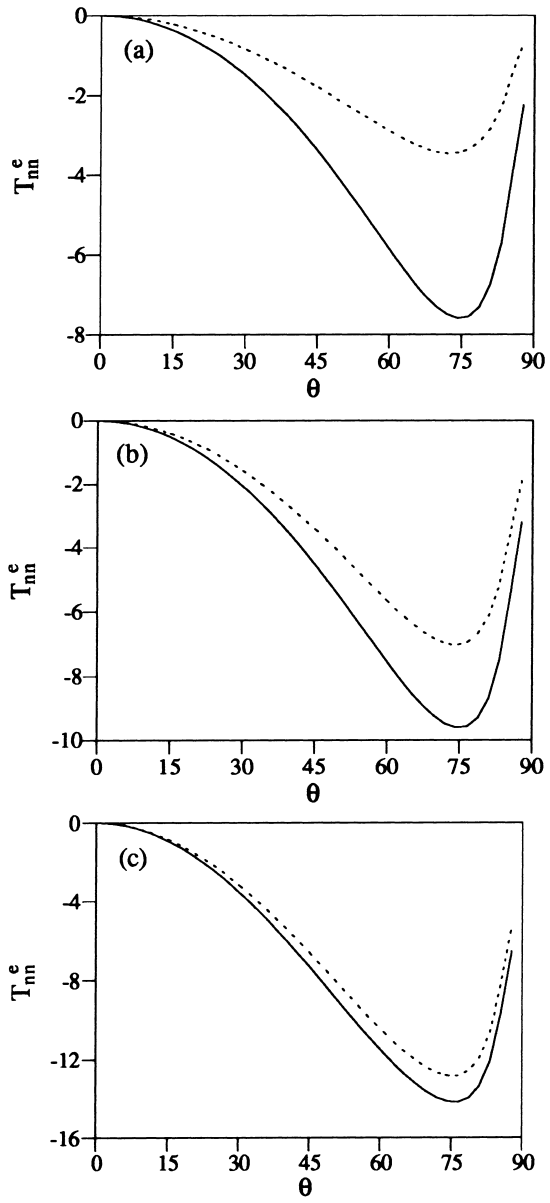

Figure 6. Comparison of the electric forces exerted on the bubble surface in the cases of conducting wall (dotted lines) and insulating wall (solid lines) (W = 3.7, R_c=0.5, N_e=0.1): (a) H = 2, (b) H = 5, (c) H = 10..

value. When $H \geq 5$, the contact angle increases almost vertically beyond a certain value of field strength. Although this has not been confirmed yet, it may be speculated that there exists no steady bubble shape beyond a certain critical value of *Ne*. This trend is even more prominent in the case of insulating bottom wall as shown in figure 13(b). Even for H = 2, we observed the same trend. This very steep increase of contact angle is due to high degree of deformation which results from the electric field concentration near the tip.

In figure 14, the relative aspect ratio $(AR)_e/(AR)_0$, where $(AR)_0$ represents the aspect ratio of the undeformed bubble in the absence of an electric field, is shown as function of *Ne* for conducting and insulating bottom walls, respectively. In the case of conducting wall(figure 14(a)), when H = 0 or H = 2, the relative aspect ratio increases almost linearly with the applied electric field strength. But, when $H \geq 5$, the relative aspect ratio increases very steeply. In the case of insulating wall (figure 14(b)), as in the case of the contact angle, steep increase of aspect ratio is observed even for small H values due to the strong nonuniform electric field near the bubble.

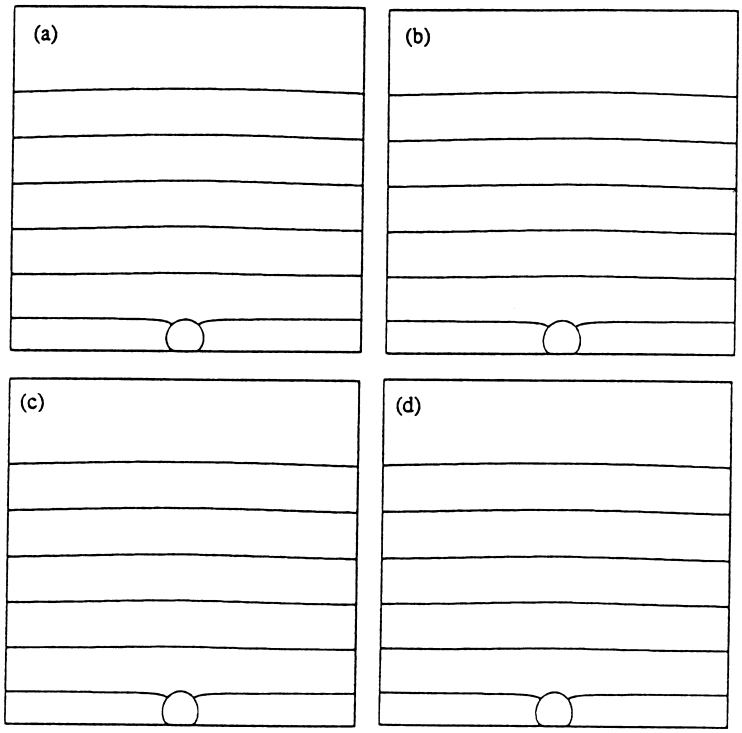

Figure 7. Numerical solutions for the shape of a bubble attached to a conducting wall ($H = 0$, $R_c = 0.5$): (a) $N_e = 0.0$, (b) $N_e = 0.6$, (c) $N_e = 0.8$, (d) $N_e = 1.0$..

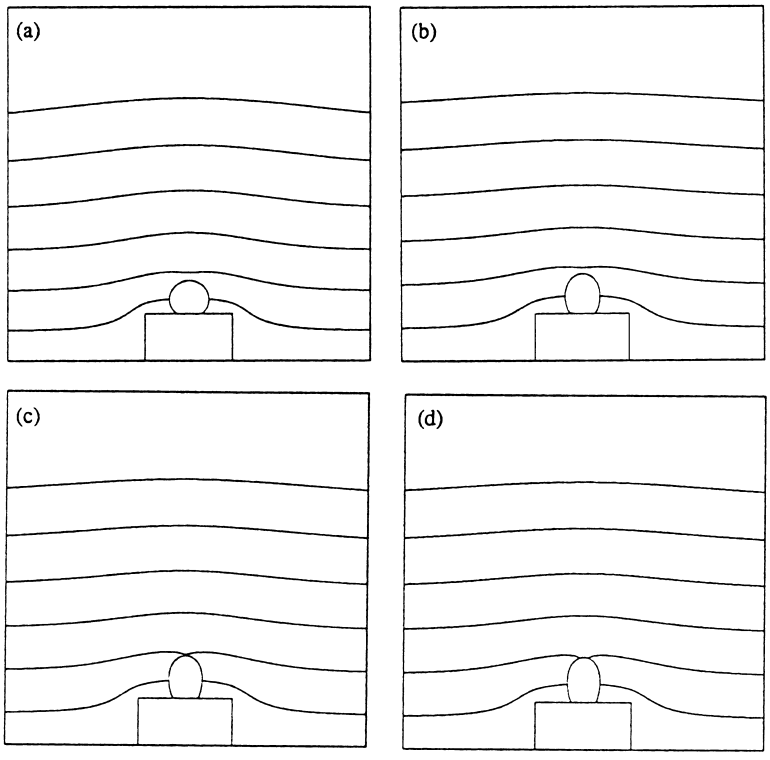

Figure 8. Numerical solutions for the shape of a bubble attached to a tip on a conducting wall ($H = 2$, $W = 3.7$, $R_c = 0.5$): (a) $N_e = 0.0$, (b) $N_e = 0.6$, (c) $N_e = 0.8$, (d) $N_e = 1.0$..

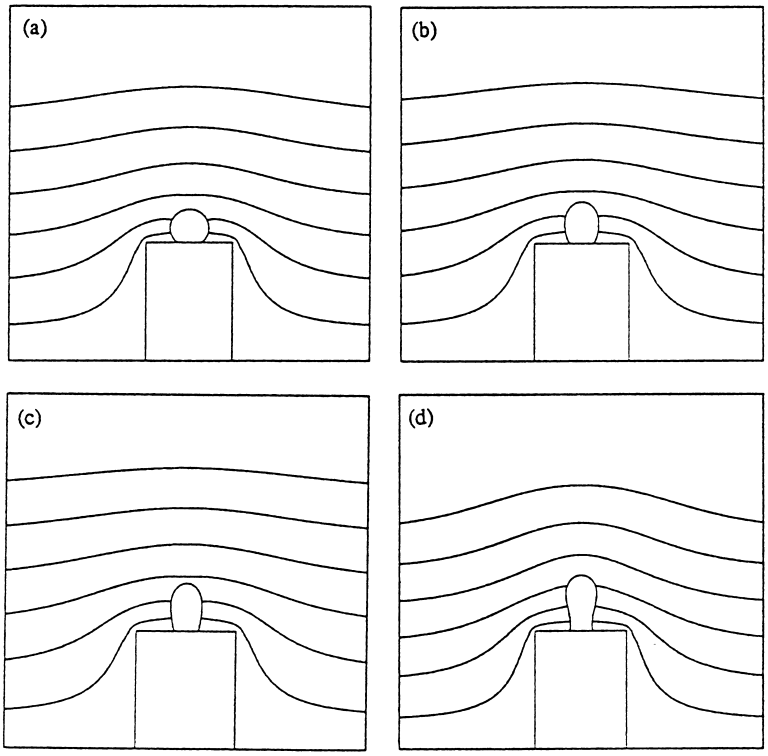

Figure 9. Numerical solutions for the shape of a bubble attached to a tip on a conducting wall ($H = 5$, $W = 3.7$, $R_c = 0.5$): (a) $N_e = 0.0$, (b) $N_e = 0.3$, (c) $N_e = 0.55$, (d) $N_e = 0.59$..

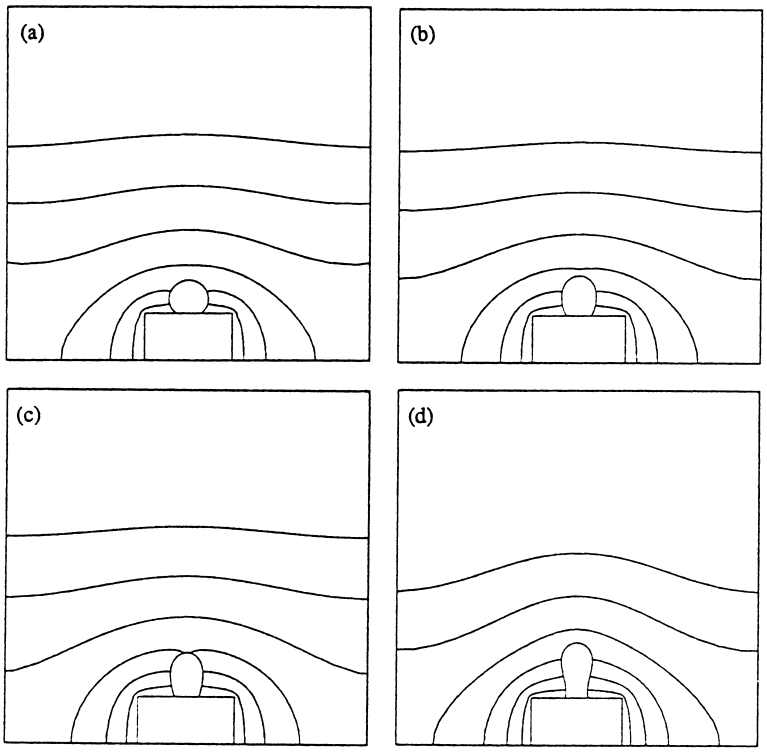

Figure 10. Numerical solutions for the shape of a bubble attached to a tip on an insulating wall ($H = 2$, $W = 3.7$, $R_c = 0.5$): (a) $N_e = 0.0$, (b) $N_e = 0.2$, (c) $N_e = 0.3$, (d) $N_e = 0.39$..

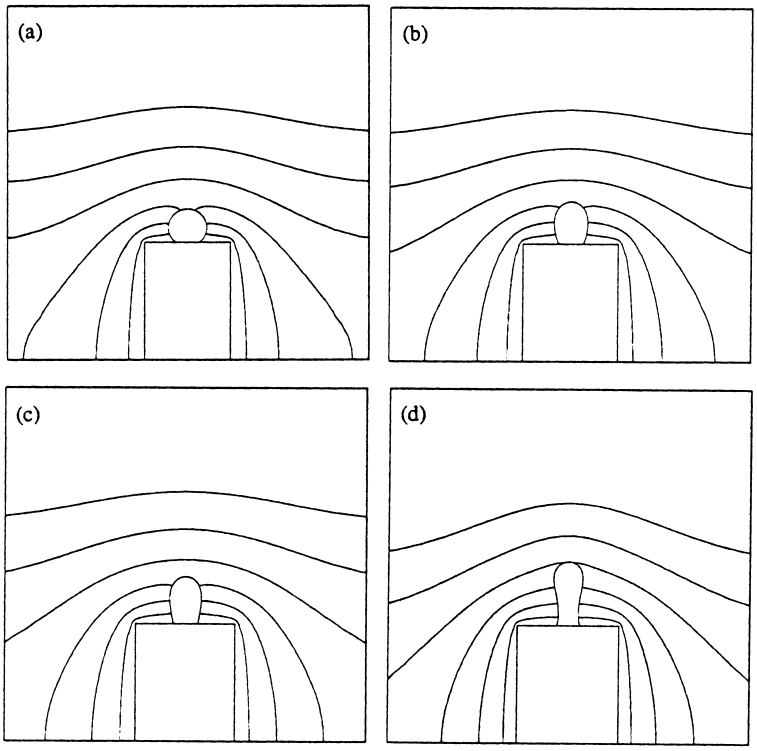

Figure 11. Numerical solutions for the shape of a bubble attached to a tip on an insulating wall ($H = 5$, $W = 3.7$, $R_c = 0.5$): (a) $N_e = 0.0$, (b) $N_e = 0.2$, (c) $N_e = 0.3$, (d) $N_e = 0.32$..

Consequently, it may be concluded that the nonuniform electric field and its intensity have significant effect on the bubble deformation.

Figure 15 shows the numerical results for the contact angle as a function of contact radius for several *Ne* values in the cases of conducting and insulating bottom walls with $H = 2$, respectively. From the figure, we can see that the contact angle increases with an increase of electric field strength under the fixed contact radius condition. From the same figure, we can also estimate the effect of an electric field on the contact radius change when the fixed contact angle condition is used. It is observed that the contact radius decreases with the increase of *Ne*. The decrease in the contact radius is much more prominent in the case of insulating bottom wall.

The bubble departure volume is also affected by the electric field. When an electric field is applied, the dimensional force balance for a bubble at departure time can be written as

$$\Delta\rho g V_d = 2\pi\gamma r_c \sin\theta_c + \int_A (-\mathbf{e}_x)\cdot(\mathbf{n}\cdot\mathbf{T}^e)\mathrm{d}A, \qquad [46]$$

where V_d and A denote the bubble departure volume and the bubble surface area at departure time. The LHS term in [46] is the $\mathbf{e}_x$ directional (upward) component of the buoyancy force, and the first and second terms in RHS are the $-\mathbf{e}_x$ directional (downward) components of the surface tension and electric forces. Hereinafter we discuss the effect of electric field on the bubble departure volume under the fixed contact angle condition as in Cheng and Chaddock (1986). As can be seen in figure 15, the contact radius decreases with an increase of electric field strength under the fixed contact angle condition. This reduction in the contact radius results in the decrease of the surface tension force between the bubble and the tip electrode. Therefore, if the $-\mathbf{e}_x$ directional (downward) force exerted on the bubble surface by the electric field exceeds the amount of decrease in the surface tension force, the departure volume increases. If an applied electric force is the same as the amount of decrease in the surface tension force, the departure volume remains unchanged. But, when the electric force is smaller than the amount of decrease in the surface tension force, the departure volume decreases.

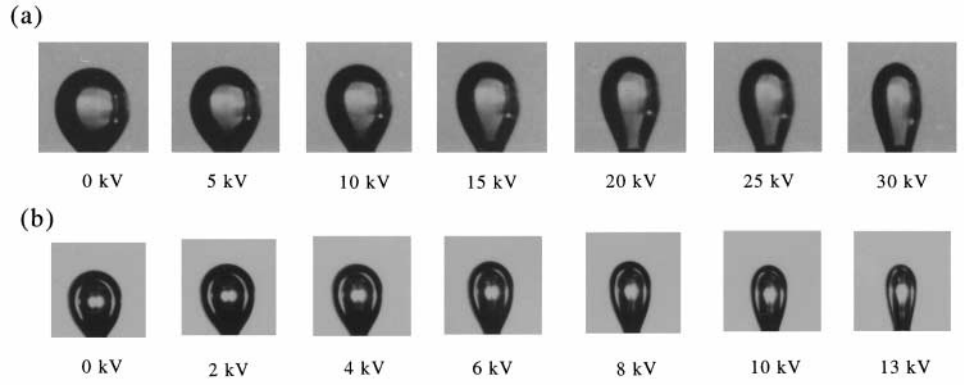

Figure 12. Experimental visualization of the shape of an air bubble attached to a needle electrode (reprinted from Kweon *et al.* 1995): (a) on a conducting plate, (b) on a teflonated plate.

In order to estimate the effect of electric field on the departure volume, we have computed the shape of a bubble in an electric field under the fixed contact angle condition. During this process, the contact radius (r_c) and the deformed bubble shape are determined to compute the surface tension force (the first term of RHS of [46]) and the $-\mathbf{e}_x$ directional electric force (the second term of RHS of [46]). Figure 16 shows the variations of the dimensionless surface

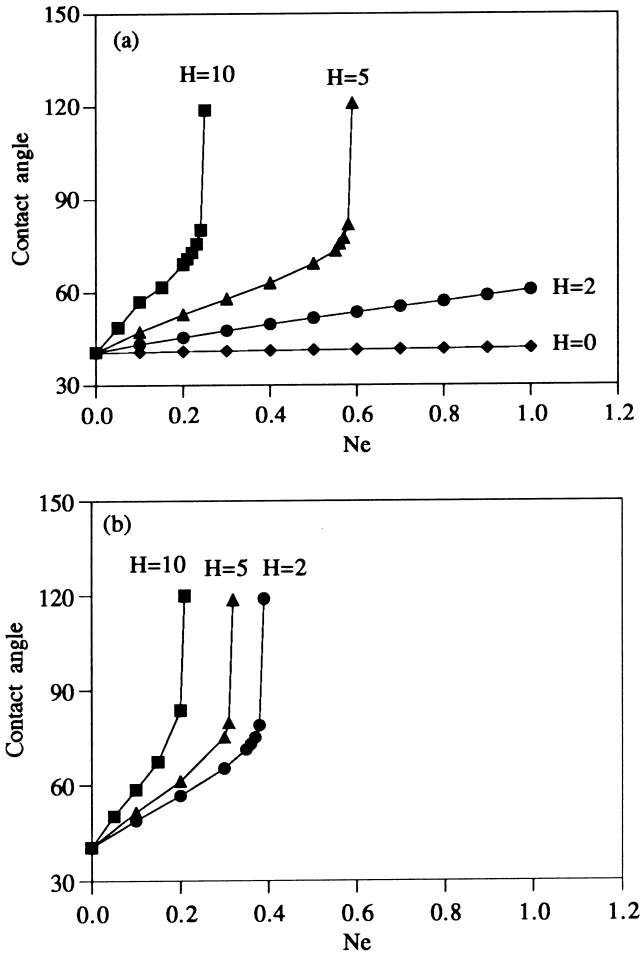

Figure 13. Numerical results for variation of the contact angle with increase of N_e for various values of H (W = 3.7, R_c = 0.5): (a) conducting wall, (b) insulating wall.

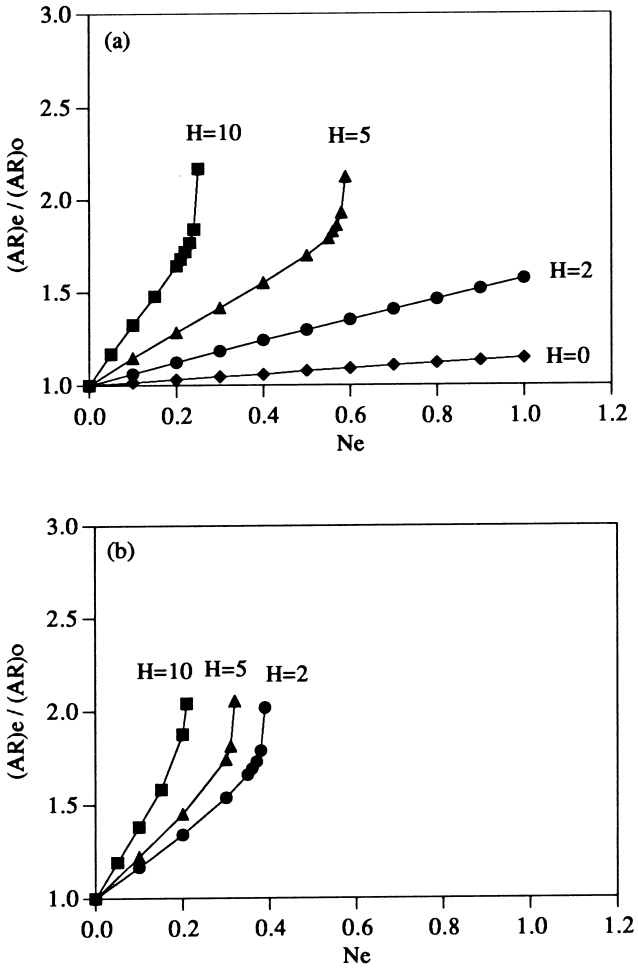

Figure 14. Numerical results for variation of the relative aspect ratio with increase of N_e for various values of H (W = 3.7, R_c = 0.5): (a) conducting wall, (b) insulating wall.

tension force and the dimensionless $-\mathbf{e}_x$ directional electric force scaled by the characteristic force scale ($F_c = \gamma a$) with the applied electric field strength when the contact angle is fixed at 60° ($\theta_c = 60°$). In the case of a conducting bottom wall, owing to the decrease in the contact radius, the surface tension force decreases with increase of *Ne* as shown in figure 16(a). When H = 0, this reduction of the surface tension force is slightly exceeded by the electric force. Therefore the $-\mathbf{e}_x$ directional net force exerted on a bubble increases very slowly with the increase of *Ne* as shown in figure 17. On the other hand, when H = 2, the downward electric force is not sufficient to make up for the decrease in the surface tension force. Thus the $-\mathbf{e}_x$ directional net force decreases with increase of *Ne* (see figure 17). In the case of an insulating bottom wall, the high degree of deformation due to the electric field concentration results in a large decrease in the surface tension forces as shown in figure 16(b). The amount of this remarkable decrease in the surface tension force is much larger than the downward electric force for conducting wall case. Therefore, the $-\mathbf{e}_x$ directional resultant force on a bubble decreases considerably with increase of electric field strength as shown in figure 17. The dimensionless downward resultant force (surface tension force plus electric force) exerted on the bubble for both types of supporting wall are summarized in figure 17.

As mentioned earlier, the effects of electric field on the departure volume can be estimated even with the results obtained for a bubble under the fixed volume condition. In figure 17, shown are the resultant dimensionless downward forces scaled by γa, where a is the character-

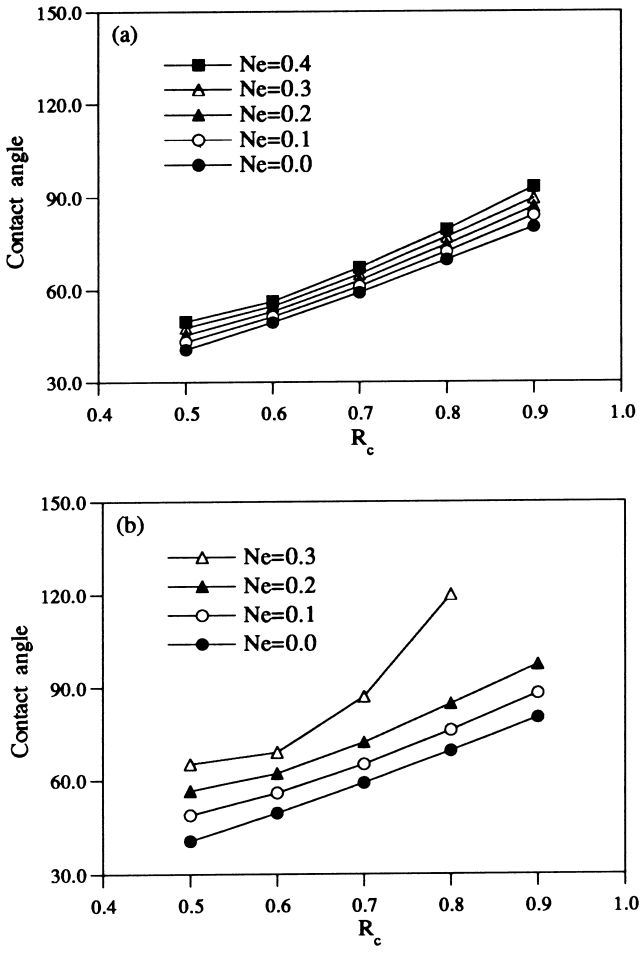

Figure 15. Plot of the contact angle vs. the dimensionless contact radius for several N_e values (H = 2, W = 3.7, R_c=0.5): (a) conducting wall, (b) insulating wall.

istic length scale. Let us assume that $l_c = a$ is the radius of the equivalent hemispherical bubble to a bubble at departure time (that is $V_d = V_0 = 2\pi a^3/3$) under the zero electric field condition. Then at this volume the LHS and the RHS of [46] are just balanced. Now, if the resultant force (surface tension force plus $-\mathbf{e}_x$ directional electric force) increases with the increase of Ne, this means that at the volume $V_0 = 2\pi a^3/3$ the RHS is larger than the LHS of [46] and that the bubble departure occurs at larger volume than the departure volume under the no electric field condition (that is $V_d > V_0$). On the other hand, if the resultant force decreases with the increase of Ne, this means that the departure volume decreases, that is V_d decreases as Ne increases. Therefore, the results in figure 17 suggest that the departure volume slightly increases with the increase of electric field strength for conducting wall without tip. This behavior has been verified by the experimental results in our previous paper (Cho *et al.* 1996). However, in the case of nonuniform electric field due to the presence of a tip, we can see that the electric field decreases the departure volume considerably. Especially, this tendency of departure volume decrease is prominent in the case of insulating bottom wall. This behavior has been well verified by the experimental observations on the bubble departure volume as shown in figure 18. In the experiment, an air bubble attached to a needle tip in cyclohexane was studied. The detailed information for the experiment has been published elsewhere (Kweon *et al.* 1995). From the figure and the numerical results, it may be concluded that the departure volume decreases as the nonuniformity of electric field increases due to the electric field concentration near the bubble.

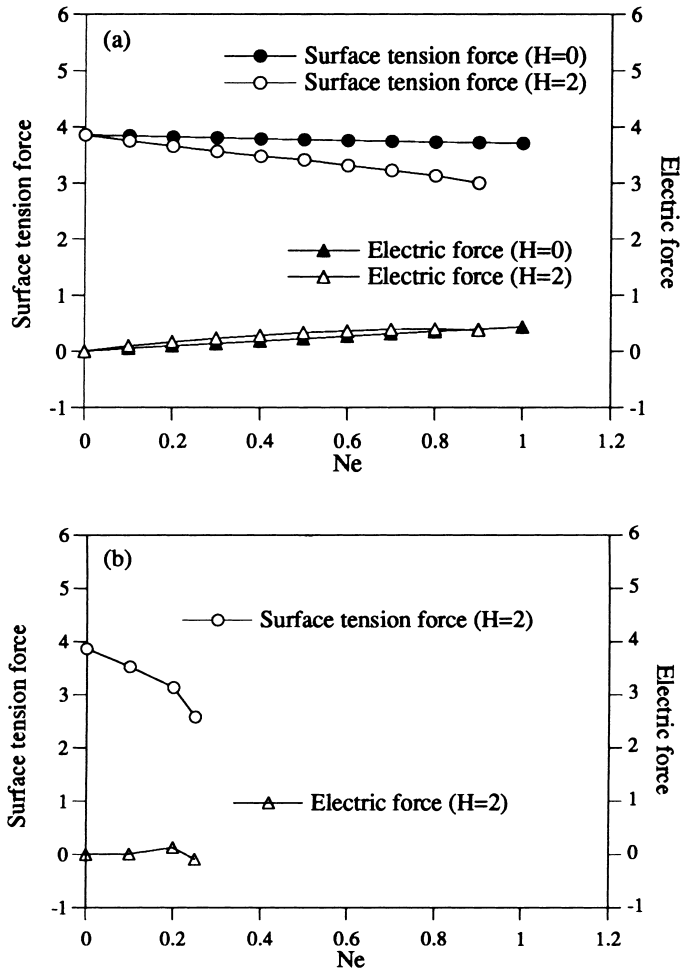

Figure 16. Numerical results for the downward surface tension and electric forces (dimensionless forces scaled by γa) exerted to a bubble of fixed reference volume under the fixed contact angle condition ($\theta_c = 60°$): (a) conducting wall, (b) insulating wall..

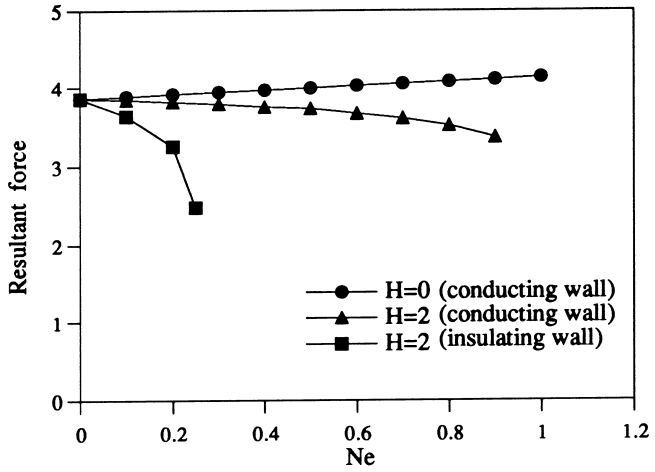

Figure 17. Numerical results for the dimensionless resultant force (surface tension force plus $-\mathbf{e}_x$ directional electric force) exerted to a bubble of fixed reference volume ($\theta_c = 60°$)..

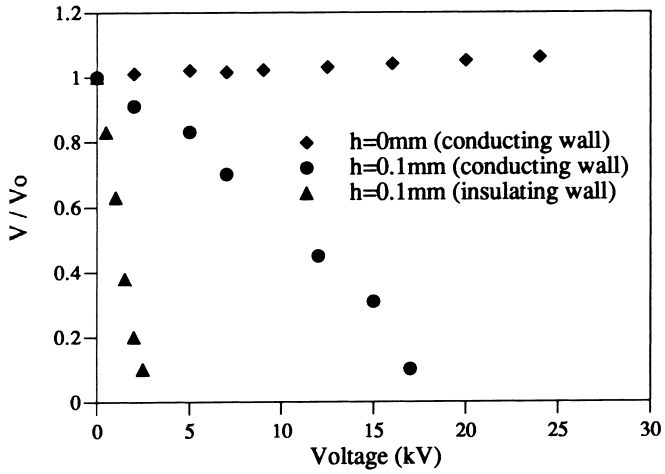

Figure 18. Experimental measurements of the relative departure volume for an air bubble attached to a needle tip in cyclohexane medium in the cases of conducting and insulating walls (detailed information on the experiment can be found from Kweon *et al.* (1995))..

5. CONCLUSION

In order to investigate the effects of a nonuniform electric field on the deformation characteristics of a bubble, numerical analyses on the steady shape of a bubble attached to a conducting tip on a supporting wall have been carried out. Two types of supporting wall are considered: a conducting and an insulating wall. From the numerical studies, we have reached the following conclusions:

(i) For both types of supporting wall, the local electric field strength near the bubble increases as the tip height increases. Therefore, the bubble elongation increases as the tip height increases. Especially in the case of insulating supporting wall, the local electric field near the bubble becomes even stronger due to the electric field concentration effect near the conducting tip. This field concentration effect due to insulating bottom wall is prominent when the tip height is small.

(ii) When the fixed contact radius condition is used, the contact angle and the relative aspect ratio increase rapidly as the strength of the applied electric field increases. The rate of increase is higher for larger value of tip height.

(iii) When the fixed contact angle condition is used, the contact radius decreases as the strength of the applied electric field increases for both types of supporting wall.

(iv) The effects of electric field on the bubble departure volume have been estimated by computing the surface tension force and the downward electric force exerted on the bubble of a fixed reference volume under the fixed contact angle condition. In the case of conducting bottom wall without tip, the downward electric force is slightly larger than the amount of decrease in the surface tension force. This fact suggests that the departure volume increases slightly with the increase of electric field strength.

(v) In the cases of nonuniform electric field due to the presence of a tip or the insulating bottom wall, the sum of surface tension force and the downward electric force decreases as the electric field strength increases. This fact suggests that the departure volume decreases with the increase of electric field strength. This tendency becomes more prominent as the tip height increases due to the electric field concentration effect.

Acknowledgements—This work was supported by the grant from the Korea Science and Engineering Foundation through the Advanced Fluids Engineering Research Center at the Pohang University of Science and Technology.

REFERENCES

Baboi, N. F., Bologa, M. K. and Klyukanov, A. A. (1968) Some feature of ebullition in an electric field. *Appl. Electr. Phenom. (USSR)* **20,** 57–70.

Batchelor, G. K. (1967) *An Introduction to Fluid Dynamics*. Cambridge University Press, Cambridge.

Berghmans, J. (1976) Electrostatic fields and the maximum heat flux. *Int. J. Heat Mass Transfer* **19,** 791–797.

Bonjour, E. and Verdier, J. (1960) Mécanisme de l'ébullition sous champ électrique. *C. R. Hebd. Seances Acad. Sci (Paris)* **,** 924–926.

Cheng, K. J. and Chaddock, J. B. (1986) Maximum size of bubbles during nucleate boiling in an electric field. *Int. J. Heat and Fluid Flow* **7,** 278–282.

Cho, H. J., Kang, I. S., Kweon, Y. C. and Kim, M. H. (1996) Study of the behavior of a bubble attached to a wall in a uniform electric field. *Int. J. Multiphase Flow* **22,** 909–922.

Choi, H. Y. (1962) Electrohydrodynamic boiling heat transfer. Ph.D. Thesis, Dept. Mech. Eng. MIT.

Cooper, P. (1990) EHD enhancement of nucleate boiling. *Trans. of the ASME* **112,** 458–464.

Crowley, J. M. (1995) Dimensionless ratios in electrohydrodynamics. In *Handbook of Electrostatic Processes*, ch. 7, 99–119. Marcel Dekker Inc., New York.

Edkie, R. G. (1976) Some experimental investigations of heat effects caused by non-uniform electric fields. *Am. Soc. Mech. Eng.* **6-WA/HT-44,** 1–8.

Fritz, W. (1935) Berechnung des Maximalvolume von Dampfblasen.*Phys. Z.* **36**, 379–388.

Jones, T. B. (1978) Electrohydrodynamically enhanced heat transfer in liquids–A Review. *Adv. Heat Transfer* **14,** 107–148.

Johnson, R. L. (1968) Effect of an electric field on boiling heat transfer. *AIAA J.* **6,** 1456–1460.

Kang, I. S. and Leal, L. G. (1987) Numerical solution of axisymmetric, unsteady free-boundary problems at finite Reynolds number I. Deformation of a bubble in a uniaxial straining flow. *Phys. Fluids* **30,** 1929–1940.

Karayiannis, T. G., Collins, M. W. and Allen, P. H. G. (1988) Electrohydrodynamic enhancement of nucleate boiling heat transfer in heat exchangers. *6th UIT Nat. Conf. Bari* 263–274.

Kweon, Y. C., Kim, M. H., Cho, H. J., Kang, I. S. and Kim, S. J. (1995) A study on the bubble deformation and departure under DC electric field. *Trans. KSME* **19,** 1518–1528.

Longuet-Higgins, M. S., Kerman, B. R. and Lunde, K. (1991) The release of air bubbles from an underwater nozzle. *J. Fluid Mech.* **230,** 365–390.

Lovenguth, R. F. and Hanesian, D. (1971) Boiling heat transfer in the presence of nonuniform direct current electric fields. *Ind. Eng. Chem. Fundam.* **10,** 570–576.

Markel, M. and Durfee, R. L. (1964) The effect of applied voltage on boiling heat transfer. *AIChE J.* **10,** 106–110.

Noh, D. S., Kang, I. S. and Leal, L. G. (1993) Numerical solutions for the deformation of a bubble rising in dilute polymeric fluids. *Phys. Fluids A* **5,** 1315–1332.

Ogata, J., Iwafuji, Y., Shimada, Y. and Yamazaki, T. (1992) Boiling heat transfer enhancement in tube-bundle evaporators utilizing electric field effects. *ASHRAE Trans.* **BA-92-5-2,** 435–444.

Ogata, J. and Yabe, A. (1993) Basic study on the enhancement of nucleate boiling heat transfer by applying electric fields. *Int. J. Heat Mass Transfer* **36,** 775–782.

Oğuz, H. N. and Prosperetti, A. (1993) Dynamics of bubble growth and detachment from a needle. *J. Fluid Mech.* **257,** 111–145.

Pohl, H. A. (1958) Some effects of nonuniform fields on dielectrics. *J. Appl. Phys.* **29,** 1182–1188.

Ryskin, G. and Leal, L. G. (1983) Orthogonal mapping. *J. Comput. Phys.* **50,** 71–100.

Ryskin, G. and Leal, L. G. (1984) Numerical solution of free-boundary problems in fluid mechanics. Part 1. The finite-difference technique. *J. Fluid Mech.* **148,** 1–17.

Schnurmann, R. and Lardge, M. G. C. (1973) Enhanced heat flux in nonuniform electric fields. *Proc. R. Soc. London Ser. A* **334,** 71–82.

Watson, P. K. (1961) Influence of an electric field upon the heat transfer from a hot wire to an insulating liquid. *Nature* **189,** 563–564.